Journal of Drug Targeting, 2011; 19(7): 562–572

ISSN 1061-186X print/ISSN 1029-2330 online
DOI: 10.3109/1061186X.2010.542243

informa
healthcare

RESEARCH ARTICLE

Thiolated polyacrylic acid-modified iron oxide nanoparticles for *in vitro* labeling and MRI of stem cells

A. Vetter[1], A. Reinisch[2], D. Strunk[2], C. Kremser[3], H. W. Hahn[4], C. W. Huck[4], T. Ostermann[5], K. Leithner[1], and A. Bernkop-Schnürch[1]

[1]Department of Pharmaceutical Technology, Institute of Pharmacy, Leopold-Franzens-University Innsbruck, Innsbruck, Austria, [2]Department of Internal Medicine, Division of Haematology, Medical University of Graz, Graz, Austria, [3]Innsbruck Medical University, Department of Radiology, Innsbruck, Austria, [4]Institute of Analytical Chemistry and Radiochemistry, Leopold-Franzens University, Innsbruck, Austria, and [5]Institute of Zoology, Leopold-Franzens University, Innsbruck, Austria

Abstract

Purpose: The purpose of this study was to develop and characterize new surface-modified iron oxide nanoparticles demonstrating the efficiency to be internalized by human endothelial progenitor cells (EPCs) from umbilical cord blood.

Methods: Iron oxide nanoparticles were coated with polyacrylic acid-cysteine (PAA-Cys) by either *in situ* precipitation or postsynthesis. The nanoparticles were characterized by X-ray powder diffraction. EPCs were labeled with PAA-Cys-modified iron oxide nanoparticles or with uncoated nanoparticles. The relaxivity of uncoated and coated iron oxide nanoparticles as well as EPCs labeled with PAA-Cys-modified iron oxide were determined.

Results: Addition of PAA-Cys increased the particle size from 10.4 to 144 and 197 nm, respectively. The X-ray powder diffraction pattern revealed that the particles consist of Fe_3O_4 with a spinal structure. Postsynthesis coated particles showed a cellular uptake of 85% and 15.26 pg iron/cell. For both types of particles the relaxivity ratio was at least 2-fold higher than that of the gold standard Resovist®.

Conclusion: The PAA-Cys coated iron oxide nanoparticles are a promising tool for labeling living cells such as stem cells for diagnostic and therapeutic application in cell-based therapies due to their high relaxivities and their easy uptake by cells.

Keywords: Stem cells, nanoparticles, iron oxide, thiomers, relaxivity

Introduction

Since the introduction of particular contrast agents in MRI use in 1987, most superparamagnetic iron oxides (SPIO) like Resovist® or Endorem®, which are taken up by macrophages, have been prepared using dextran or other types of polymer coatings to achieve good dispersion in water (Molday and MacKenzie, 1982). Iron oxide particles such as magnetite ($Fe^{II}(Fe^{III})_2O_4/Fe_3O_4$) or its oxidized form maghemite (γ-Fe_2O_3) are by far the most commonly employed for biomedical applications (Kim et al., 2007).

Their utilization in stem cell transplantation is a powerful treatment method for many diseases. In leukemia treatment, SPIOs particles are coupled to stem cells to provide essential information about the migration behavior of the transplanted cells in the host organism. Therapeutic stem cells that are labeled to permit cell tracking hold promise for answering questions about the optimum timing of administration, cell location, and cell viability over time. Surface modification of iron oxide is a key goal to enhance its permeability into cell membranes. Biocompatible polymers and targeting agents are therefore attached to nanoparticle surfaces to make them more biocompatible and to increase their nonspecific intracellular

Address for Correspondence: A. Bernkop-Schnürch, Department of Pharmaceutical Technology, Institute of Pharmacy, Leopold-Franzens-University Innsbruck, Innrain 52, Josef Möller Haus, 6020 Innsbruck, Austria. E-mail: Andreas.Bernkop@uibk.ac.at

(Received 07 June 2010; revised 14 November 2010; accepted 18 November 2010)

uptake (Zhang and Zhang, 2005; Allen et al., 2004). Furthermore, one of the difficulties of synthesizing iron oxides is the intrinsic agglomeration of magnetic nanoparticles. The formed aggregates are then quickly sequestered by cells of the reticular endothelial system. To avoid macrophage recognition particles are surface-protected by a layer of hydrophilic groups (Fan et al., 2007). In different studies, magnetic nanoparticles have been coated with surfactants or polymers to overcome these problems (Horak et al., 2007). Thiolated polymers such as poyacrylic acid-cysteine might also be a useful tool for increasing the intracellular uptake because of (i) surface stabilization of nanoparticles via disulfide bonding (Loretz et al., 2007); (ii) thiol-functions which react with the outer cell surface leading to an improved absorptive endocytocis (Martien et al., 2007); and (iii) comparatively low toxicity (Vetter et al., 2010). Furthermore, it is possible to avoid macrophage recognition by PAA-Cys coated iron oxide nanoparticles without influencing stem cell uptake.

The objective of this study is to develop a new type of iron oxide nanoparticle that utilizes ferumoxides-polyacrylic acid-cysteine complex (PAA-Cys) as a prospective particle for transport into cells and subsequently for magnetic cell labeling. Since Fourier Transform Infrared (FT-IR) spectroscopy was introduced as fast and non-invasive tool for particle investigation and derivatization (Heigl et al., 2008) this technique was performed to investigate the synthesis of the newly developed nanoparticles. Furthermore, the synthesized Fe_3O_4-polyacrylic acid-cysteine complexes (PAA-Cys) were investigated by their particle characterizations and particle structure, their iron content and their relaxation rates compared to the magnetic resonance contrast agent Resovist®. Moreover, the percentage of the labeled human endothelial progenitor cells (EPCs) from umbilical cord blood and long-term viability were evaluated.

Materials and methods

Materials

Polyacrylic acid solution in water, MW 100 (35 wt.%), (1-ethyl-3-(3-dimethylaminopropyl)carbodiimide hydrochloride) (EDAC), L-cysteine free base, Ellman's reagent (DTNB, 5,5'-dithiobis(2-nitrobenzoic acid)), 2,4,6-trinitrobenzenesulfonic acid (TNBS) were obtained from Sigma-Aldrich, Vienna, Austria.

For cell culture preparation medium, penicillin/streptomycin solutions were purchased from PAA Pasching, Austria. 12-well cell culture plates were purchased at Corning, Acton, MA. Endothelial cell growth medium-2 (EGM-2) was obtained from Lonza, Walkersville, MD. Heparin 5000 IE/ml was purchased from Biochrom AG Seromed, Berlin, Germany. EPCs from umbilical cord blood and pooled human platelet lysate (pHPL) were obtained from Medical University of Graz, Department of Internal Medicine, Division of Haematology, Graz, Austria. *In vitro* stem cell studies were approved by the local ethical committee (ethical committee Medical University Graz).

All other chemicals were of reagent grade and obtained from Sigma, Vienna, Austria.

Polymer synthesis

The polyacrylic acid 100-cysteine conjugate (PAA-Cys) was synthesized according to a method described previously by our research group (Bernkop-Schnürch et al., 1999). In brief, cysteine was covalently attached to PAA via the formation of amide bonds between the primary amino group of cysteine and a carboxylic acid group of the polymer. The carboxylic acid moieties of 2.8 g of polymer in 100 ml of demineralised water were activated for conjugation by the addition of EDAC in a final concentration of 50 mM. After 15 min 1 g of L-cysteine hydrochloride was added and the pH-value of the reaction mixture was adjusted to six. Reaction mixtures were stirred and incubated at room temperature for 3 h. Resulting conjugates were isolated by dializing against 5 l of 0.2 mM HCl two times, additionally two times against 5 l of 0.2 mM HCl containing 1% NaCl and again two times against 5 l of 0.2 mM HCl in 5 l distilled water.

After dialysis protected from light at 4°C to avoid oxidation of thiol moieties, the resulting polymer-cysteine conjugate was adjusted to pH 4.0 and lyophilised by drying frozen aqueous polymer solutions at −75°C condenser temperature at 4×10^{-4} mbar (VirTis, Gardiner, ME). Preceding freeze drying, the polymer was frozen at −70°C (REVCO, Knoxville, TN). Polymer conjugate was stored at 4°C until further use.

Degree of thiolation of the polymer conjugates

The amount of free thiol groups immobilized on the polymer backbone, i.e. the degree of modification, was determined photometrically with Ellman's reagent quantifying free thiol groups (Ellman, 1958). The total amount of sulfhydryl groups fixed on the polymer, represented by the summation of free thiol groups and of oxidized thiol moieties available in form of disulphide bonds was quantified with Ellman's reagent after reduction with $NaBH_4$ (Habeeb, 1973).

Preparation of uncoated iron oxide nanoparticles

Maghemite was synthesized according to a method described previously (van Ewijk et al., 1998). Magnetite was precipitated by dissolving 3.26 g of $FeCl_2 \times 4\ H_2O$ and 8.70 g of $FeCl_3 \times 6\ H_2O$ in 380 ml demineralized water and adding 20 ml of 25% NH_3 to this solution while stirring vigorously. After sedimentation the precipitate with a centrifuge (14,000 rpm for 5 min), the supernatant was removed by decantation. 40 ml 2 M HNO_3 was then added to the black sediment and the mixture was stirred for 5 min. The oxidation to magnetite was completed by adding 60 ml 0.35 M $Fe(NO_3)_3$ to the mixture and stirring it at its boiling temperature for 1 h. After sedimentation and washing with 2 M HNO_3, the reddish yellow sediment was dispersed in demineralized water.

Postsynthesis coating with polyacrylic acid-cysteine

Nanoparticles were formed spontaneously due to the addition of magnetite. For this purpose PAA-Cys (1 mg/ml w/v) was dissolved in distilled water and the pH of the solutions was adjusted to 7.0 with 1 M sodium hydroxide. Afterwards, 10 mg/ml magnetite was dissolved in distilled water. Finally, 1 ml of the iron oxide solution was added to 10 ml of the PAA-Cys solution under magnetic stirring at room temperature for 90 min.

In situ encapsulation of iron oxide in polyacrylic acid-cysteine solution

Cysteine was covalently attached to PAA via the formation of amide bonds between the primary amino group of cysteine and a carboxylic acid group of the polymer. Therefore, the carboxylic acid moieties of 2.8 g of polymer in 100 ml of demineralised water were activated for conjugation by the addition of 1 g of EDAC, the pH was adjusted to 6 with 5 M NaOH and 30 ml of a suspension of the produced magnetite (10 mg/ml) were added. After 15 min 1 g of L-cysteine hydrochloride was added and the pH-value of reaction mixture was adjusted to six. Reaction mixtures were stirred and incubated at room temperature for 3 h. Resulting conjugates were isolated by dializing against 0.2 mM HCl two times, additionally two times against 0.2 mM HCl containing 1% NaCl and again two times against 0.2 mM HCl. After dialysis protected from light at 4°C to avoid oxidation of thiol moieties, pH of the resulting Fe_3O_4-polymer-cysteine conjugate suspension was adjusted to 7.0.

Size determination of the particles (ESI/EELS)

The hydrodynamic diameters of the produced nanoparticles (50 μg/ml) were measured by photon correlation spectroscopy (PCS) using a PSS NICOMP™ 380 DLS/ZLS (Santa Barbara, CA) with a 7.5 mW laser diode at 635 nm. The measurements were carried out at room temperature with a scattering angle of 90. To verify the results obtained by PCS, energy filter transmission electron microscopy (EFTEM) of the nanoparticles was performed. Nanoparticles were adsorbed on carbon-coated copper grids and examined with a Zeiss Libra 120 EFTEM at 80 kV. Image analysis was achieved using Olympus SiS iTEM 5.0 and TRS 2048 high speed camera. Electron energy loss spectroscopy (EELS) and electron spectroscopic imaging (ESI) were utilized for qualitative and quantitative element analysis. Therefore, nanoparticles were selected at magnification ×31,500 and EEL-spectra were measured from 690 to 750 eV.

ESI was carried out using a three window method from 660 to 718 eV to obtain finally a computer generated element distribution.

Visualization of nanoparticles at high magnification was accomplished with high contrast imaging at 250 eV. HC-images were inverted for comparison with conventional transmission electron microscopic images and the net distribution of iron was overlaid.

Electrokinetic potential

The zeta potential of nanoparticles was measured (incubated for 30 min at 37°C). The zeta potential was analysed by measuring the electrophoretic mobility using a PSS NICOMP™ 380 DLS/ZLS. All measurements were carried out at room temperature.

Content determination of iron in coated-PAA-Cys and uncoated PAA-Cys particles

The total iron content of an iron oxide-PAA-Cys nanoparticles suspension and uncoated iron oxide nanoparticles suspension was important for calculation of adjacent MR relaxivities and was determined by inductively coupled plasma spectroscopy, Jobin Yvon JY38 PLUS, Germany (plasma P1 12 l/min, coatergas G1 0.3 l/min, nebulizer 0.2–0.4 bar). The amount of iron was calculated by interpolation from an appropriate external standard curve.

Particle structure analysis of iron oxide nanoparticles

X-ray powder diffraction using a AXS-Bruker D8 diffractometer, Bruker, Germany (Cu-target (wavelength $CuKa_{1,2}$: 0.15406 nm), E-dispersive counter, parallel beam optics, theta/theta coupled, 9 position sampler changer) was used to identify the structure of the uncoated nanoparticles. Standard operating conditions: 40 kV, 40 mA, contineous scan 2–70° theta/2theta, step size 0.02 steps, counting time 8 s, room conditions.

FT-IR-ATR analysis

The binding of PAA-Cys to iron oxide in a solid sample of iron oxide-PAA-Cys was checked using a Spectrum 100 system, purchased from Perkin Elmer (Vienna, Austria). The Spectrum software, version 6.3.1, used for recording and manipulation the spectra, was also from Perkin Elmer. The spectrum was recorded in over the range of 4000–750 cm^{-1}. All samples were dried under vacuum before measurements using an Eppendorf concentrator 5301 (Eppendorf, Hamburg, Germany). Synthesized uncoated iron oxide nanoparticles were additionally washed four times with water to remove remaining traces of HNO_3, then dried and analyzed.

Cell culture

Frozen EPCs from human umbilical cord blood were diluted immediately in EGM-2 supplemented with 2 mmol/l l-glutamine 100 U/ml penicillin, and 100 μg/ ml streptomycin. Fetal bovine serum was replaced by 10% pHPL to create a humanized culture system that may be translated into medically relevant applications (Reinisch, 2009; Schallmoser et al., 2007). The pHPL was prepared from pooled platelet-rich plasma derived from a minimum of 40 whole blood donations as previously reported (Schallmoser et al., 2007). Heparin 5000 IE/ml were added. Cells were seeded at a density corresponding to 100–500 cells/cm^2 in well-plates and cultured at 5% CO_2, 37°C, 95% air humidity. Nonadherent cells were removed by complete change of medium after 2–3 days. The medium was changed every 5 days as the cells grew to

confluence. The cells were lifted by incubation with 0.25 wt % trypsin.

Quantitative analysis of labeled cells

EPCs were plated on uncoated 12-well culture plates. PAA-Cys-modified iron oxide nanoparticles were added to the culture medium (100 µg/ml) for 72 h. After the iron oxide nanoparticles were washed out of the culture medium with 0.1 M phosphate-buffered saline, the cells were fixed with 4% paraformaldehyde and stained for iron with 2% potassium ferrocyanide and 1% hydrochloric acid at a ratio 1:1 to produce ferric ferrocyanide (Prussian blue). A counterstain was accomplished with nuclear fast red solution. Labeled and unlabeled cells were quantified using an inverted light microscope (Motic AE31, Neukirchen, Germany) by counting randomly five fields per well and two wells per each run. The cells captured on each image were manually labeled as Prussian blue positive or negative; the labeled cells were then counted.

Cytotoxicity tests

MTT assay

The medium was replaced by 1 ml (100 µg/ml) uncoated and coated iron oxide nanoparticles in sterilized water, respectively, using culture medium by itself as control. After 4-h incubation solutions were removed and each well was treated with 1 ml of 3-(4,5-dimethylthiazol-2-yl)-2,5-diphenyltetrazolium bromide solution (0.6 mg MTT/ml) in EGM-2 medium and incubated at 37°C in a humidified atmosphere of 5% CO_2/95% O_2 for further 2 h. Then, MTT solution was replaced by 1 ml per well of acidic isopropanol (0.04 M HCl in absolute isopropanol) in order to dissolve the formazane crystals. The dye solution with the nasal cells was centrifuged at 13,000 rpm for 2 min (Sigma 3–18 centrifuge). The absorbance of the supernatant was measured at a wavelength of 570 nm with backround subtraction at 650 nm with Tecan infinite M200 spectrophotometer, Grödig, Austria.

LDH test

Cell viability was determined by measuring lactate dehydrogenase (LDH) activity in the incubation medium with a spectrophotometer at 490 nm. The cell culture medium was replaced by 1 ml (100 µg/ml) uncoated and coated iron oxide nanoparticles in sterilized water. Cells incubated with culture medium served as negative control. Next, 200 µl aliquots of incubation medium were collected every hour over a time periode of 4 h and incubated with 100 µl of cytotoxicity Detection Kit reaction mixture (Roche Diagnostics, Meylan, France) for 30 min at room temperature in the dark. LDH activity in the incubation medium was compared with that measured after complete lysis of the cells in medium containing 2% (v/v) Triton X-100 (high control).

The apparent cytotoxicity was calculated according to the following equation:

$$\text{Cytotoxicity}\,(\%) = \frac{\text{triplicate absorbance} - \text{low control}}{\text{high control} - \text{low control}} * 100 \quad (1)$$

MR relaxometry and MR imaging of Fe_3O_4 modified and unmodified nanoparticles and labeled cells

MR imaging was performed on a standard 1.5 T clinical whole-body MR system (Magnetom Avanto, Siemens, Germany). For relaxivity measurements a linearly polarised loop receiver coil was used (inner diameter 60 mm). MR relaxivity measurements were performed on serial dilutions of the coated and uncoated nanoparticles in distilled water. The individual solutions were filled into 500-µl tubes (Eppendorf AG, Germany) and placed within the MRI receiver coil using a special sample holder. T1 measurements were performed using an inversion recovery snapshot FLASH sequence (TR = 3.6 ms, TE = 2.1 ms, flip angle 8°, receive bandwidth 490 Hz/pixel, FOV 67 mm, acquisition matrix 64·128, 1 slice, slice thickness 5 mm) with multiple inversion times (TI = 140, 200, 400, 600, 800, 1000, 1200, 1500, 1700, 2000, 2500, 3000, 3500, 4000 ms). T2 measurements were performed using a CPMG-type multi-echo spin-echo (SE) sequence (TR = 1000 ms, TE = n·13.5 ms with $n = 1...16$, receive bandwidth = 130 Hz/pixel, FOV = 51 mm, acquisition matrix = 128 × 128, 1 slice, slice thickness = 3 mm). T1 and T2 parameters were calculated by a two-parameter fit to the obtained signal intensities.

Furthermore, the relaxivity of cell suspensions with different concentrations of cells labeled with uncoated and coated iron oxide nanoparticles was investigated. For this purpose, suspensions of cells labeled with PAA-Cys-modified iron oxides or with uncoated iron oxide nanoparticles in 4% gelatin were prepared. MR relaxation measurements were performed as described above.

Iron analysis

The amount of iron in the cells after mineralization was determined by spectrophotometry. Cell containing samples were mineralized by the addition of 4.5 ml HCl (25%) in an ultrasonic bath (50°C, 15 min). Deionized water and one drop of lanthanum nitrate was added to reach a total volume of 5 ml. The iron content was determined using an atom absorption spectrophotometer (Philips PU 9100, Germany). The measurements were repeated three times and the mean value was determined.

Statistical data analysis

Statistical data analysis was performed using the Student's *t*-test with $p < 0.05$ and $p < 0.005$ as the minimal level of significance, respectively.

Results

Characterization of the PAA-Cys conjugate

The amount of free thiol groups and disulphide bonds distributed all over the polymeric network of the

polyacrylic acid-cysteine conjugate was quantified via Ellman's reagent. The PAA-Cys conjugate used in this study displayed 381.26 ± 33.38 µmol thiol groups per gram polymer. Furthermore, 160.0 ± 37.71 µmol disulphide bonds per gram polymer could be quantified (means ± SD, $n = 3$). In addition, quantification of the remaining primary amino groups on the polyacrylic acid-cysteine conjugate was carried out with TNBS according to the method described previously by our research group (Bernkop-Schnürch and Krajicek, 1998). This indicated that no remaining free unconjugated cysteine remained in the sample. The fact that the PAA-Cys conjugate displays no primary amino groups while displaying thiol moieties provides strong evidence for the formation of amide bonds between the polymer and cysteine. The lyophilized polymer was white, odorless and of fibrous structure. It became swollen quickly in water.

Nanoparticle preparation and characterization

Iron oxide colloids were prepared by two methods: (i) precipitation of iron oxide during the synthesis of polyacrylic acid-cysteine solution (*in situ* coating) and (ii) precipitation followed by oxidation to magnetite and addition of polyacrylic acid-cysteine solution (postsynthesis coating). Generally, iron oxide cores were prepared by precipitation of iron salts, particularly $FeCl_2 * 4\ H_2O$ $FeCl_3 * 6\ H_2O$, by increasing the pH followed by oxidation with $Fe(NO_3)_3$. Oxidation resulted in magnetite (Fe_3O_4). Furthermore, the stabilizer polyacrylic acid-cysteine was used to protect the iron oxide cores from aggregation and to improve particle stability and cell uptake. Shape and size of the magnetic nanoparticles obtained both *in situ* and postsynthesis coating were analysed via EFTEM. These microscopic images of the synthesized magnetic particles showed relatively high uniformity in terms of size and spherical shape with a rather narrow size distribution (Figure 1A–3A) of 10.4 nm. Nanoparticles also showed a typical iron Fe $L_{2,3}$ edge using EELS. Furthermore, ESI showed the net distribution of iron and computer generated overlays confirmed that the element is located within the postsynthesis and *in situ* coated nanoparticles (Figure 1B, d-3b, d). EEL-spectrum of magnetite nanoparticles gave a typical Fe peak at 708eV (Figure 1C–3C). The reference EEL-spectrum in Figure 4 shows a typical Fe $L_{2,3}$ peak.

Table 1 shows the dependence of the hydrodynamic particle diameter, measured by dynamic light scattering for freshly prepared iron oxide nanoparticles. The hydrodynamic size is larger than the size obtained by EFTEM which was investigated in further studies (Horak et al., 2007). The hydrodynamic size of coated particles increased by 1.7 and 2.3 times due to a thickening of the shell. *In situ* coated nanoparticles showed a 1.4 increase in particle size in contrast to postsynthetically coated particles. This may be due to the coating process itself. The size calculated from PCS was 14 and 19 times larger than that from TEM, mainly due to the effect of large particles on the hydrodynamic diameter (Horak et al., 2007).

The zeta potential of postsynthesis coated Fe_3O_4 nanoparticles was 1.4-fold higher than that of *in situ* coated nanoparticles. The coated colloids did not precipitate at neutral pH. The stability can be ascribed to the negative charges of the shell whereas postsynthesis coated particles showed a higher stability than *in situ* encapsulated ones. The total iron content in 1 ml of iron nanoparticle suspension varied with the type of coating. The content of iron in uncoated nanoparticle suspension is 13 times higher than that of postsynthesis coated particles and 5 times higher than that of *in situ* coated nanoparticles.

Figure 5 shows the X-ray powder diffraction pattern for uncoated nanoparticles. There are seven characteristic reflexes of 4.82, 2.92, 2.53, 2.09, 1.71, 1.61, and 1.48 Å. These results revealed that the particles are pure Fe_3O_4 with a spinal structure. Additionally, the average diameter of the crystals (in nanometers) was calculated with the program TOPAS 2.1 (Bruker). The average particle size of Fe_3O_4 was 10.4 ± 0.2 nm which is in accordance with the observations from EFTEM.

Surface modification of magnetic nanoparticles was or monitored by FT-IR-ATR spectroscopy. The IR spectral measurements are shown in Figure 6A–6d. In detail, iron oxide nanoparticles (Figure 6A) and PAA-Cys polymer (Figure 6B) were recorded and characteristic absorptions were observed for the polymer. The investigations of *in situ* coated and postsynthesis coated iron oxide particles are depicted in Figure 6C and 6D. Characteristic absorptions at following wave lengths were determined

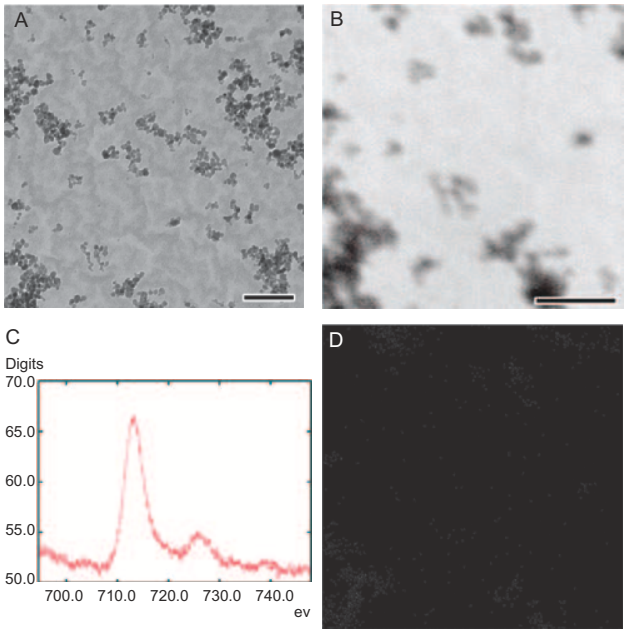

Figure 1. (A) Transmission electron microscopic image of uncoated magnetite nanoparticles agglomerate. Magnification 31,500×. Scale bar 100 nm. (B) Detail of nanoparticles using energy filters: Inverted high contrast image at 250 eV, and computer generated iron (Fe) distribution overlaid in red. Scale bar 50 nm. (C) EEL-spectrum of uncoated magnetite nanoparticles showing a typical Fe peak at 708 eV. (D) Net distribution of iron shown with electron spectroscopic imaging (ESI) of nanoparticles.

indicating the functional groups C-H (2900 cm^{-1}), S-H (2570 cm^{-1}), C=O (1700 cm^{-1}), C-N (1180 cm^{-1}) and C-S (800 cm^{-1}) all demonstrating the presence of PAA-Cys being attached to the nanoparticles surface.

Quantitative analysis of labeled cells

Cell labeling with iron oxide nanoparticles is a common method for *in vivo* cell monitoring, as the labeled cells can be detected by magnetic resonance imaging (Babic et al., 2008). Human EPCs labeled with either uncoated or surface-modified iron oxide nanoparticles were observed using an inverted light microscope (Figure 7A–7C). Using the Prussion Blue reaction, the cellular iron content was measured in EPCs exposed to the nanoparticles. Observations revealed the iron oxide nanoparticles as dark dots in EPCs. Cells endocytosed ~36% of uncoated Fe_3O_4 nanoparticles (Figure 7D). Cells in contact with PAA-Cys modified nanoparticles took up to 73% and 85% of iron oxide-PAA-Cys nanoparticles (Figure 7D), respectively. Hence, a significantly larger percentage ($p < 0.5$) of cells was labeled with coated than with uncoated nanoparticles. Particles coated with post-synthesis nanoparticles appeared to adhere to the cell walls. This was indicated by the fact that the blue-stained areas were larger than the cells (Figure 7C) (Babic et al., 2008).

Cytotoxicity tests

Cell viability, determined by the ability of the cells to metabolically reduce MTT to a formazan dye, was performed after a 4-h exposure to uncoated and coated iron oxide particles. The results from the MTT assay and LDH test are shown in Figures 8 and 9. Viability of EPCs labeled

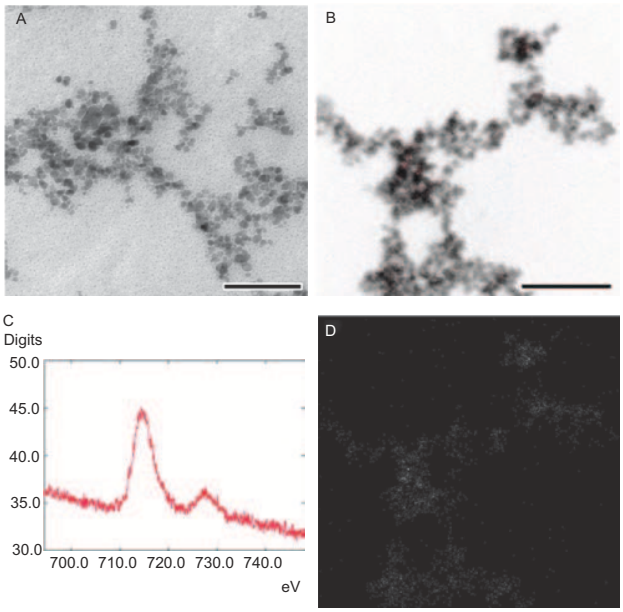

Figure 2. (A) Transmission electron microscopic image of postsynthesis coated magnetite-PAA-Cys modified nanoparticles agglomerate. Magnification 31500×. Scale bar 100 nm. (B) Detail of nanoparticles using energy filters: Inverted high contrast image at 250 eV, and computer generated iron (Fe) distribution overlaid in red. Scale bar 50 nm. (C) EEL-spectrum of postsynthesis coated magnetite-PAA-Cys modified nanoparticles showing a typical Fe peak at 708 eV. (D) Net distribution of iron shown with electron spectroscopic imaging (ESI) of nanoparticles.

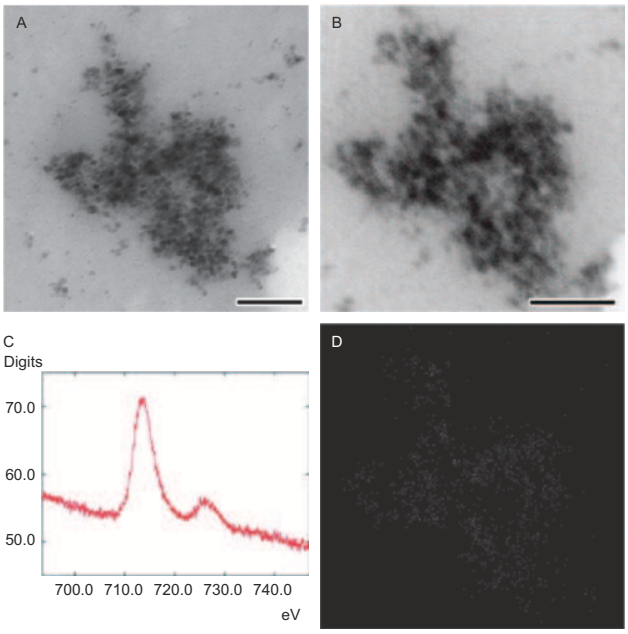

Figure 3. (A)Transmission electron microscopic image of in situ magnetite-PAA-Cys modified nanoparticles agglomerate. Magnification 31500×. Scale bar 100 nm. (B) Detail of nanoparticles using energy filters: Inverted high contrast image at 250 eV, and computer generated iron (Fe) distribution overlaid in red. Scale bar 50 nm. (C) EEL-spectrum of in situ magnetite-PAA-Cys modified nanoparticles showing a typical Fe peak at 708 eV. (D) Net distribution of iron shown with electron spectroscopic imaging (ESI) of nanoparticles.

Table 1. Sizes and zeta potentials of iron oxide particles measured as hydrodynamic diameters by PCS and total iron content (means ± SD, $n = 3$).

Iron oxide nanoparticles	Particle size (nm) mean of Gaussian distribution in distilled water	Zeta potential (mV) mean of Gaussian distribution in distilled water	Total iron content (mg/ml)
uncoated Fe_3O_4	86.7 ± 9.9	−0.62 ± 0.8	13.65 ± 0.20
PAA-Cys-Fe_3O_4 (postsynthesis coating)	144.1 ± 15.7	−13.6 ± 5.1	1.02 ± 0.03*
PAA-Cys-Fe_3O_4 (coating during the synthesis)	197.2 ± 7.3	−9.7 ± 2.5*	2.87 ± 0.07*

*Differs from uncoated Fe_3O_4 with $p < 0.005$.

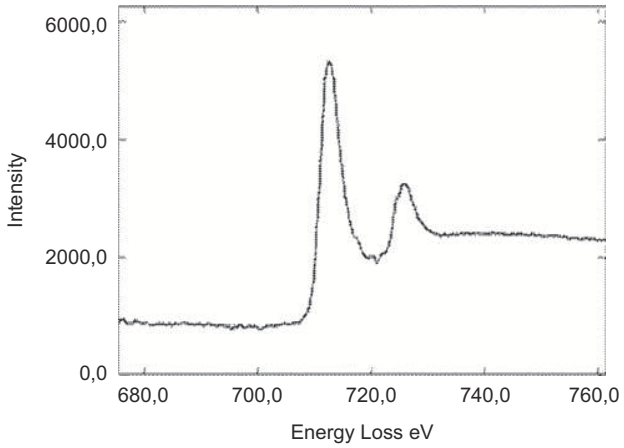

Figure 4. Reference EEL-spectrum of iron showing a typical Fe L2,3 peak at 708 eV.

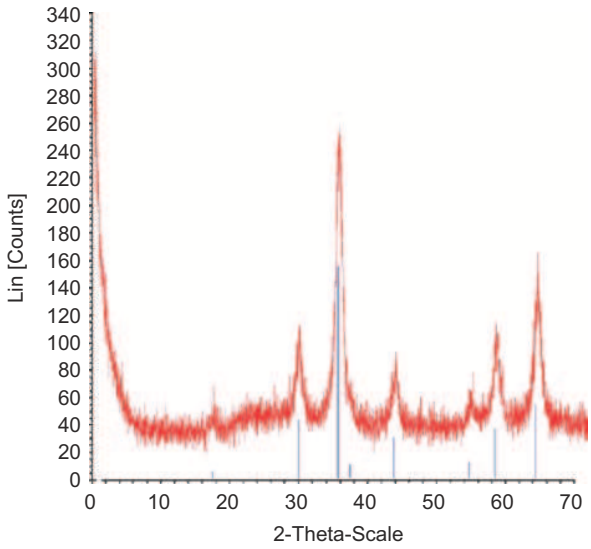

Figure 5. X-ray analysis of uncoated nanoparticles. Vertical bars: Fe_3O_4 standard.

with uncoated iron oxide nanoparticles was almost 94%. Accordingly, PAA-Cys has an impact on the EPCs depending on the method of coating. *In situ* coated iron oxide nanoparticles showed a significant ($p < 0.005$) difference on the viability of EPCs in comparison to uncoated ones. Almost 87% of EPCs labeled with postsynthesis coated particles survived within the observation period of 4 h. Just about 78% of EPCs labeled with *in situ* coated particles were viable. Uncoated Fe_3O_4- or Fe_3O_4-PAA-Cys-induced cytotoxicity based on quantifying the release of LDH from membrane-damaged cells was measured after 0, 1, 2, 3, and 4 h of exposure. A 1- to 4-h exposure to *in situ* coated γ-Fe_2O_3 showed the most appreciable effect on LDH release with around 17% from EPCs. EPCs treated with postsynthesis coated Fe_3O_4 in LDH test were associated with a slighter decrease in viability and integrity. They showed cytotoxicity in the range of 13%. Furthermore, uncoated Fe_3O_4 nanopartciles induced 14% of cell death.

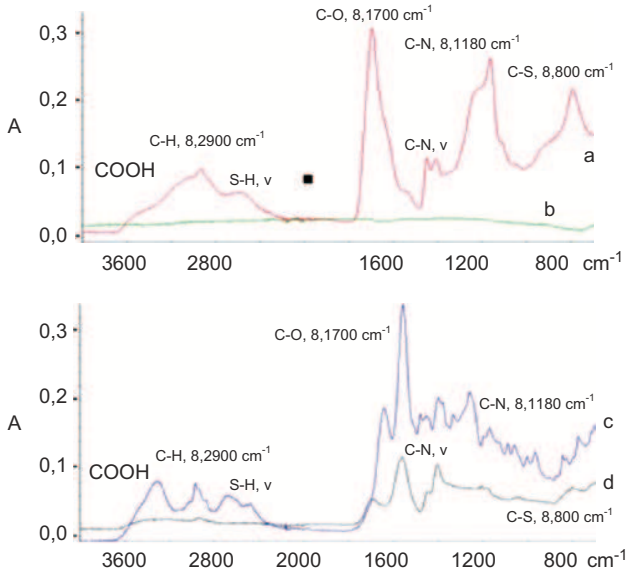

Figure 6. FT-IR-ATR spectra of iron oxide particles before and after surface modification: spectrum of pure PAA-Cys polymer (A), uncoated iron oxide particles (B), *in situ* coated particles (C), and postsynthesis coated particles (D).

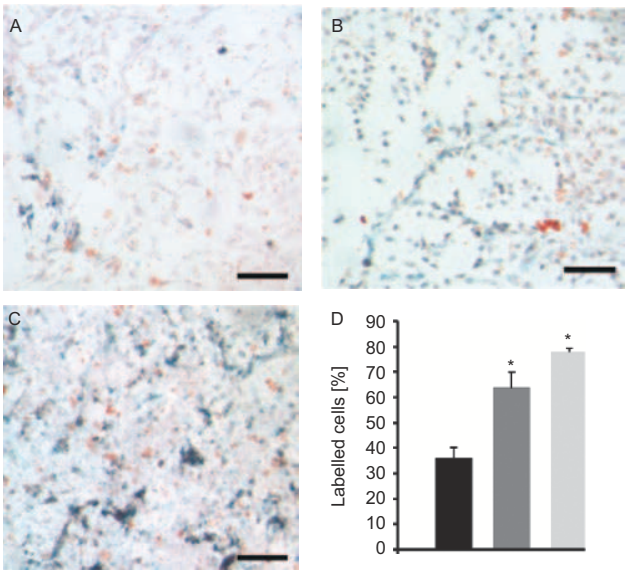

Figure 7. Microscopic image of EPCs labeled with (A) uncoated iron oxide nanoparticles, (B) *in situ* magnetite-PAA-Cys modified nanoparticles, and (C) postsynthesis coated magnetite-PAA-Cys modified nanoparticles. Scale bar 200 nm. (D) Histograms of the percentage of the Prussian blue stained uncoated (black column), *in situ* coated (dark gray column) and postsynthesis coated (light gray column) iron oxide nanoparticle-labeled EPC cells, (means ± SD, $n = 4$). *) differs from uncoated Fe_3O_4 with $p < 0.005$.

MR relaxometry

Figure 10 shows the dependence of the MR relaxation rates R_1 and R_2 as a function of the iron concentration in distilled water. The slope of the obtained curves thereby represents the relaxivities of the contrast agent r_1 and r_2, respectively. The obtained relaxivity values are summarized in Table 2. Compared to the commercially available

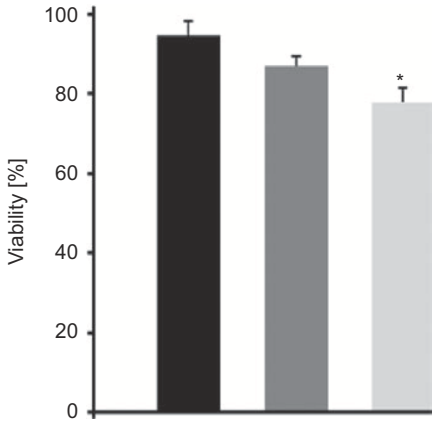

Figure 8. Comparison of the viability of uncoated (black column), *in situ* coated (light gray column) and postsynthesis coated (dark gray column) iron oxide nanoparticles on EPC cell culture (means ± SD, $n = 3$). *) differs from uncoated Fe_3O_4 with $p < 0.05$.

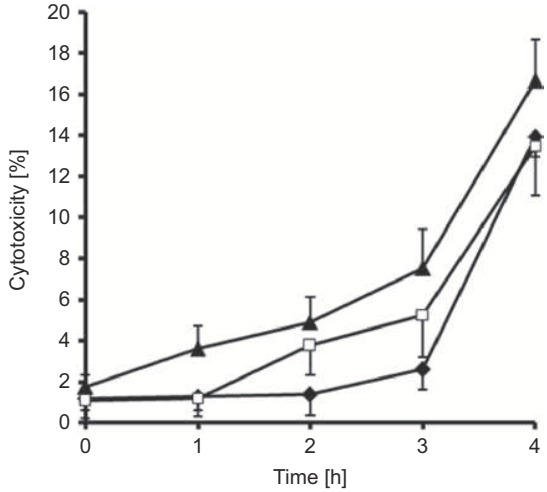

Figure 9. Results from the LDH test of uncoated (◆), *in situ* coated (▲) and postsynthesis coated (□) iron oxide nanoparticles on EPC cell culture (means ± SD, $n = 3$).

nanoparticulate iron oxide agent Resovist® the r_1 relaxivity of nanoparticles was two- to three-fold lower, whereby the highest r_1 value was found for the postsynthesis coated nanoparticles and the lowest value for the uncoated nanoparticles. For the coated nanoparticles the r_2 relaxivity was comparable to that of Resovist®, while for the uncoated nonparticles the r_2 value was four-fold lower. r_1 varied only by a factor of about 1.5 between the different coated nanoparticles, whereas the r_2 variation was ~3.5-fold. For all nanoparticles the ratio r_2/r_1 was considerably larger than 1 which is typical for superparamagnetic contrast agents (Koenig and Kellar, 1995). For the *in situ* coated nanoparticles the ratio r_2/r_1 was highest, followed by the postsynthesis coated nanoparticles, where both showed an at least two-fold higher ratio than Resovist®. Figure 11 shows the dependence of the MR relaxation rates R_1 and R_2 after uptake of the nanoparticles into EPCs as a function of the total iron concentration in the samples. The relaxivities obtained from the slope of the

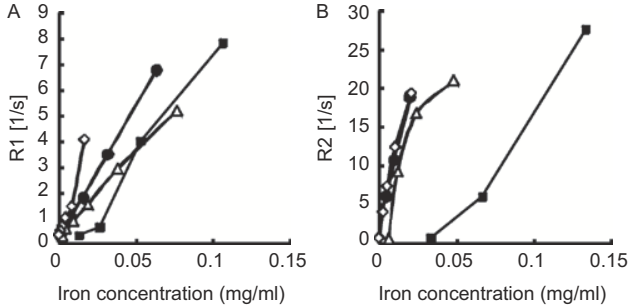

Figure 10. Proton relaxation rates (A) R1 and (B) R2 of serial dilutions of uncoated (■), *in situ* coated (Δ), postsynthesis coated (•) iron oxide nanoparticles and ResovistR (◊).

curves are summarized in Table 2. The highest relaxivity both for r_1 and r_2 is found for the postsynthesis coated nanoparticles. Uncoated nanoparticles again show the lowest relaxivities. r_1 relaxivities for all nanoparticles were decreased after uptake into EPCs, whereas r_2 was increased for the uncoated und postsynthesis coated nanoparticles and considerably decreased for the *in situ* nanoparticles. For r_1 only a minor difference was found between postsynthesis and *in situ* coated particles and for r_2 almost no difference was found between uncoated and *in situ* coated particles.

Iron analysis

The average amounts of iron determined by spectrophotometry after mineralization were 1.94 pg iron per cell for cells labeled with uncoated iron oxide particles, 15.26 pg iron per cell for postsynthesis coated iron oxide particles and 9.47 pg iron per cell for *in situ* coated iron oxide particles.

Discussion

Due to its biocompatibility and strong effects on T2(*) relaxation, iron oxide nanoparticles are currently the MR contrast agent of choice for cell labeling. Several methods have been described that shuttle sufficient amounts of iron oxide into cells. Polyacrylic acid has been used to stabilize magnetic nanoparticles by providing electrostatic and steric repulsion (Lin, et al., 2005).

The size of the particles measured by techniques such as EFTEM or XRD (X-Ray Diffraction) varies from one agent to another and is generally between 4 and 10 nm (Jung and Jacobs, 1995). In this study the average particle size of the Fe_3O_4 core was 10.4 ± 0.2 nm. The size of the particles themselves with their coating varies more widely and the method of measurement significantly contributes to this variability. The hydrodynamic diameter of Resovist® coated with carboxydextran, for instance, is 60 nm. Endorem® coated with Dextran T10 ranges between 120 and 180 nm (Corot et al., 2006). In this study, the hydrodynamic diameter of the coated particles varied depending on the coating method. Conversely, Horak et al. (Horak et al., 2007) report of the smaller size of *in situ* prepared nanoparticles than postsynthesis coated

Table 2. MR relaxivities on serial dilutions of the coated and uncoated nanoparticles in distilled water and MR relaxivities of cell suspensions with different concentrations of cells labeled with uncoated and coated iron oxide nanoparticles related to the iron content in mg/ml.

Serial dilutions of nanoparticles	r_1 (ml/mg s)	r_2 (ml/mg s)	r_2/r_1
Uncoated iron oxide nanoparticles	84	692	8.24
In situ coated nanotarticles	65	2140	32.92
Postsynthesis coated nanoparticles	102	2476	24.27
Resovist®	216	2778	12.86
Cell suspensions with nanoparticles	r_1 (ml/mg s)	r_2 (ml/mg s)	r_2/r_1
Uncoated iron oxide nanoparticles	29	1229	41.9
Postsynthesis coated nanoparticles	48	2955	61.9
In situ coated nanoparticles	44	1437	32.8

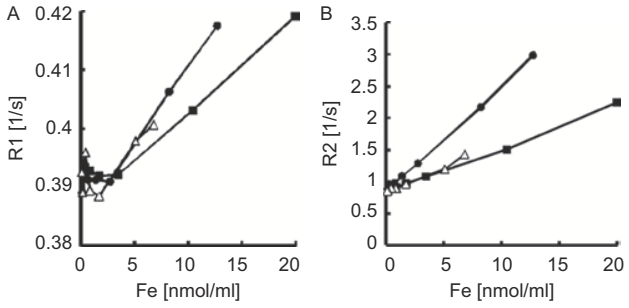

Figure 11. Proton relaxation rates (A) R1 and (B) R2 of uncoated (■), *in situ* coated (Δ) and postsynthesis coated (•) iron oxide nanoparticles taken up by endothelial progenitor cells (EPC) as a function of the total iron concentration. Varying iron concentration thereby represents a varying number of cells within the individual samples.

ones. The smaller size was due to the coating agent d-mannose during precipitation, which interfered with the nucleation step of iron oxide formation resulting in a smaller size compared with the postsynthesis method in which the coating was applied to existing particles. However, in this study the coating of iron oxide colloidal nanoparticles was achieved by a different *in situ* coprecipitation method.

Furthermore, the zeta potential is an important parameter as it can influence particle stability. The negative charge of Fe_3O_4-PAA-Cys is likely based on the carboxyl groups of PAA-Cys.

FT-IR-ATR spectroscopy confirmed the surface modification of iron oxide nanoparticles with PAA-Cys. Higher signal intensity could be observed after *in situ* coating compared to postsynthesis coating. This can be explained by a higher polymer amount on the particles surface. Furthermore, FT-IR spectra indicate the presence of abundant pendent carboxyl groups in the structure particularly of *in situ* prepared nanoparticles. During the preparation process, some of the pendent carboxyl groups may form strong chelating bonds with ferric or ferrous ions and provide the nucleation point for iron oxide formation. At the same time, the highly branched polymer chains may limit the growth of the iron oxide crystals and block the aggregation of crystals (Ma et al., 2007). Furthermore, Sreeram et al. (2004) determined that the interaction between the polymer alginate and iron ions could be explained by a site-binding model, i.e. iron ions are bound to binding sites in the alginate and form spatially separated iron ion centers on the alginate backbone. Furthermore, Liao and Chen (2002) depicted that uncoated PAA was covalently bound onto iron oxide nanoparticles via carbodiimide activation. In addition, the polymer chains would also help to stabilize the whole particle. One reason for the improved stability of Fe_3O_4-PAA-Cys may be the binding of the carboxyl groups of PAA-Cys to iron oxide nuclei. Ma et al. (2007) assumed that the COO^- terminal of alginate coordinates to Fe of Fe_3O_4 by complex formation. Fe_3O_4 nanoparticles were bound with alginate and this interaction might be as strong as a hydrogen bond, which also explains the high stability of SPION-alginate.

Postsynthesis coated nanoparticles provided a lower stability by addition of high concentrations of iron oxide due to the appearance of precipitation. Therefore, better intercalation of the iron oxide particles was achieved by the *in situ* coating technique. Ma et al. (2007) calculated that a suspension sample of SPION-alginate comprised a Fe_3O_4 concentration of 1–4 mg/ml when prepared with alginate at concentrations of 1–4% (m/m). In contrast the commercial magnetite nanoparticles Resovist® and Endorem® exhibit a total iron content of 28 and 11.2 mg/ ml, respectively.

The surface characteristics of nanoparticles plays an important role for their uptake into cells. Approximately three in every ten cells in contact with the uncoated nanoparticles or 1.94 pg as determined by spectrophotometry endocytosed iron oxide. This might be explained by the formation of aggregates of sterically unstable particles (Babic et al., 2008). In an attempt to increase cell labeling, the iron oxide surface was modified with PAA-Cys. PAA-Cys is a polyanion due to the presence of carboxylic acid groups which also offer the advantage that sulfhydryl moieties of cysteine can be easily attached to such polymers via the formation of amide bonds (Bernkop-Schnürch, 2005). The uptake of postsynthesis and *in situ* coated nanoparticles did not differ significantly but postsynthesis coated nanoparticles also adhered to the cell walls as it was investigated by Babic et al. (Babic et al., 2008). In further studies (Horak et al., 2007; Babic et al., 2008) even a relatively low concentration of coating agent was sufficient for almost complete cell labeling. Here, 87.5% of human mesenchymal stem cells and 92.2% of rat bone marrow stromal cells were labeled with poly(l-lysine) solution coated iron oxide nanoparticles (Babic et al., 2008). Furthermore, 80.6% of rat bone marrow stromal cells were labeled with postsynthesis d-mannose coated iron oxide nanoparticles (Horak et al., 2007). A

higher concentration of the coating agent d-mannose results in an increased viscosity promoting particle aggregation and adhesion to the cell surface (Horak et al., 2007). Hence, postsynthesis coated nanoparticles may show a higher cell labeling rate and iron amount per cell in contrast to *in situ* coated ones due to a lower amount of PAA-Cys.

The mechanism responsible for the more efficient uptake of coated nanoparticles may be due to the anionic charge provided by carboxyl groups and the sulfhydryl groups in PAA-Cys. Here, the thiol-reactive functions present at the surface of the nanoparticles could react covalently with the cells outer surface and this interaction could lead to an absorptive endocytosis and surface stabilized nanoparticles (Loretz et al., 2007; Martien et al., 2007). The cell uptake of the anionic nanoparticles can also be due to an endocytosis as a two step method: first a nonspecific binding step to the cellular membrane mainly due to electrostatic interactions and second an internalization step (Wilhelm et al., 2003).

In this study, the coating method had an effect on the EPC cells. Results of these examinations were in accordance with other studies. Liu et al. (2009), for instance, showed that cell viability of human nasopharyngeal epidermal carcinoma cells (KB cells) still remains above 90% when they were incubated with magnetite particles of different concentrations for 6 h. Thiomers per se did not lead to a remarkable mortal effect after incubation on human nasal epithelial cells (Vetter et al., 2010). Therefore, in case of *in situ* encapsulated iron oxide nanoparticles the slightly decreased viability could be trace back to the production process itself.

MR relaxation properties of SPIO nanoparticles are usually explained by the so called outer-sphere relaxation process which is based on the diffusion of water protons within the inhomogeneous magnetic field created by the nanoparticles (Koenig and Kellar, 1995) and on an additional Curie contribution which is based on magnetic field fluctuations due to macromolecular motion (Roch et al., 1999). Theory predicts for the high frequency regime (magnetic field strengths >1T) a decrease of r_1 relaxivity, going gradually to zero, whereas the r_2 relaxivity stays at comparably high values, leading to a high r_2/r_1 value, as seen for our nanoparticles. Furthermore, it is also shown that the relaxivity is sensitive to particle size. In this study, a small variation of r_1 but a strong variation of r_2 with particle size was found, which is in accordance with work of Morales (2003). This is also reflected in an increase of the ratio r_2/r_1 with increasing particle size, which is interpreted as an indication of outer-sphere relaxation effect (Morales, 2003). Size effects as predicted by theory (Roch et al., 1999) usually only consider the size of the iron core. Since for nanoparticles the size of the iron core was found constant for the different preparations the obtained dependence of relaxivity on particle size most probably reflects the influence of coating, which on one hand is expected to influence the macromolecular motion of the particles and on the other hand the accessibility of water protons to the iron core. The influence of iron core size is reflected by the fact that coated iron oxide nanoparticles with a core size of 10.4 nm had a considerably higher r_2/r_1 ratio compared to Resovist® with an iron core size of 4.2 nm. In addition to the above effects, r_2/r_1 is also influenced by iron core composition. Crystalline paramagnetic inclusions (uncoupled Fe^{3+} ions and/or isolated Fe^{3+} ions bound to coating) (Bulte et al., 1999) can reduce r_2/r_1 which might explain the lower r_1 and r_2 relaxivity for the *in situ* coated nanopartcles in this study.

Finally, a change of relaxivities after uptake of nanoparticles into EPC's was observed. Similar changes were observed by Simon et al. (2006), who investigated just one sort of dextran coated iron oxide nanoparticles. From the data it is seen that the amount of relaxivity change obviously depends on the nature of surface coating, where uncoated and postsynthesis coated nanoparticles showed an increase of relaxivity and *in situ* coated nanoparticles showed a strong decrease of relaxivity. These findings suggest that the nature of surface coating influences intracellular interactions and thus as for example, macromolecular motion of the nanoparticles which, as discussed above, is an important factor for relaxivity (Roch et al., 1999).

It has been shown that magnetic particles are physiologically well tolerated and that the surface of the particles is responsible for the biocompatibility and stability to the reticulo-endothelial system (Berry, 2005). Both *in vitro* and *in vivo* biocompatibility of PAA have also been demonstrated in previous studies (Ghavamzadeh et al., 2004). Bioavailability of magnetic nanoparticles for MR imaging is also a key factor of a potent delivery system. Babic et al. (2008), for instance, showed that poly(l-lysine)- modified iron oxide labeled stem cells injected intracerebrally were clearly discernible *in vivo* by MRI even at low concentrations.

Conclusion

New surface-modified iron oxide nanoparticles were produced by two different methods. The surface of the magnetic nanoparticles was modified by polyacrylic acid-cysteine and the particles were characterized by several methods to confirm that PAA-Cys successfully coated the particles. The structure of the polymer shell of the iron oxide core determined the efficacy of the nanoparticles interaction with the cells. Compared to the uncoated iron oxide nanoparticles, both the higher ratio r_2/r_1 of postsynthesis PAA-Cys-modified nanoparticles and their better uptake in the cells enabled easier MRI detection and tracking of stem cells after transplantation. Therefore, the developed nanoparticles may be a promising tool for the invasive *in vivo* tracking of transplanted cells in the host organism and for monitoring the long-term effects of such transplantations.

Acknowledgements

The Austrian-Nano-Initiative cofinanced this work as part of the Nano-Health Project. The authors wish to thank Peter Rutzinger from the Institute of Analytical Chemistry and Radiochemistry, University of Innsbruck for accomplishment of the iron content determinations into the cells.

Declaration of interest

The authors report no conflicts of interest. The authors alone are responsible for the content and writing of the paper.

References

Molday RS, MacKenzie D. (1982). Immunospecific ferromagnetic iron-dextran reagents for the labeling and magnetic separation of cells. J Immunol Methods, 52, 353–367.

Kim D, Hong KS, Song J. (2007). The present status of cell tracking methods in animal models using magnetic resonance imaging technology. Mol Cells, 23, 132–137.

Zhang Y, Zhang J. (2005). Surface modification of monodisperse magnetite nanoparticles for improved intracellular uptake to breast cancer cells. J Colloid Interface Sci, 283, 352–357.

Allen MJ, MacRenaris KW, Venkatasubramanian PN, Meade TJ. (2004). Cellular delivery of MRI contrast agents. Chem Biol, 11, 301–307.

Fan QL, Neoh KG, Kang ET, Shuter B, Wang SC. (2007). Solvent-free atom transfer radical polymerization for the preparation of poly(poly(ethyleneglycol) monomethacrylate)-grafted Fe3O4 nanoparticles: synthesis, characterization and cellular uptake. Biomaterials, 28, 5426–5436.

Horak D, Babic M, Jendelová P, Herynek V, Trchová M, Pientka Z, Pollert E, Hájek M, Syková E. (2007). D-mannose-modified iron oxide nanoparticles for stem cell labeling. Bioconjug Chem, 18, 635–644.

Loretz B, Thaler M, Bernkop-Schnürch A. (2007). Role of sulfhydryl groups in transfection? A case study with chitosan-NAC nanoparticles. Bioconjug Chem, 18, 1028–1035.

Martien R, Loretz B, Thaler M, Majzoob S, Bernkop-Schnürch A. (2007). Chitosan-thioglycolic acid conjugate: an alternative carrier for oral nonviral gene delivery? J Biomed Mater Res A, 82, 1–9.

Vetter A, Martien R, Bernkop-Schnürch A. (2010). Thiolated polycarbophil as an adjuvant for permeation enhancement in nasal delivery of antisense oligonucleotides. J Pharm Sci, 99, 1427–1439.

Heigl N. (2008). When size matters near infrared reflection spectroscopy of nanostructured materials. J Near Infrared Spec, 16, 211–221.

Bernkop-Schnürch A, Schwarz V, Steininger S. (1999). Polymers with thiol groups: a new generation of mucoadhesive polymers? Pharm Res, 16, 876–881.

Ellman GL. (1958). A colorimetric method for determining low concentrations of mercaptans. Arch Biochem Biophys, 74, 443–450.

Habeeb AF. (1973). A sensitive method for localization of disulfide containing peptides in column effluents. Anal Biochem, 56, 60–65.

van Ewijk GA, Vroege GJ, Philipse AP. (1998). Convenient preparation methods for magnetic colloids. J Magnetism and Magnetic Materials, 201, 31–33.

Reinisch A. (2009). Humanized large-scale expanded endothelial colony–forming cells function *in vitro* and *in vivo*. Blood, 113, 6716–6725.

Schallmoser K, Bartmann C, Rohde E, Reinisch A, Kashofer K, Stadelmeyer E, Drexler C, Lanzer G, Linkesch W, Strunk D. (2007). Human platelet lysate can replace fetal bovine serum for clinical-scale expansion of functional mesenchymal stromal cells. Transfusion, 47, 1436–1446.

Bernkop-Schnürch A, Krajicek ME. (1998). Mucoadhesive polymers as platforms for peroral peptide delivery and absorption: synthesis and evaluation of different chitosan-EDTA conjugates. J Control Release, 50, 215–223.

Babic M, Horák D, Trchová M, Jendelová P, Glogarová K, Lesný P, Herynek V, Hájek M, Syková E. (2008). Poly(L-lysine)-modified iron oxide nanoparticles for stem cell labeling. Bioconjug Chem, 19, 740–750.

Koenig SH, Kellar KE. (1995). Theory of 1/T1 and 1/T2 NMRD profiles of solutions of magnetic nanoparticles. Magn Reson Med, 34, 227–233.

Lin CL, Lee CF, Chiu WY. (2005). Preparation and properties of poly(acrylic acid) oligomer stabilized superparamagnetic ferrofluid. J Colloid Interface Sci, 291, 411–420.

Jung CW, Jacobs P. (1995). Surface properties of superparamagnetic iron oxide MR contrast agents: ferumoxides ferumoxtran ferumoxsil. Magn Reson Imaging, 13, 675–691.

Corot C, Robert P, Idée JM, Port M. (2006). Recent advances in iron oxide nanocrystal technology for medical imaging. Adv Drug Deliv Rev, 58, 1471–1504.

Ma HL, Qi XR, Maitani Y, Nagai T. (2007). Preparation and characterization of superparamagnetic iron oxide nanoparticles stabilized by alginate. Int J Pharm, 333, 177–186.

Sreeram KJ, Yamini Shrivastava H, Nair BU. (2004). Studies on the nature of interaction of iron(III) with alginates. Biochim Biophys Acta, 1670, 121–125.

Liao MH, Chen DH. (2002). Preparation and characterization of a novel magnetic nano-adsorbent. J Mater Chem, 12, 3654–3659.

Bernkop-Schnürch A. (2005). Thiomers: a new generation of mucoadhesive polymers. Adv Drug Deliv Rev, 57, 1569–1582.

Wilhelm C, Billotey C, Roger J, Pons JN, Bacri JC, Gazeau F. (2003). Intracellular uptake of anionic superparamagnetic nanoparticles as a function of their surface coating. Biomaterials, 24, 1001–1011.

Liu J, Sun Z, Deng Y, Zou Y, Li C, Guo X, Xiong L, Gao Y, Li F, Zhao D. (2009). Highly water-dispersible biocompatible magnetite particles with low cytotoxicity stabilized by citrate groups. Angew Chem Int Ed Engl, 48, 5875–5879.

Roch A, Muller RN, Gillis P. (1999). Theory of proton relaxation induced by superparamagnetic particles. J Chem Phys, 110, 5403–5411.

Morales MP. (2003). Contrast agents for MRI based on iron oxide nanoparticles prepared by laser pyrolysis. J Magn Magn Mater, 266, 102–109.

Bulte JW, Brooks RA, Moskowitz BM, Bryant LH Jr, Frank JA. (1999). Relaxometry and magnetometry of the MR contrast agent MION-46L. Magn Reson Med, 42, 379–384.

Simon GH, Bauer J, Saborovski O, Fu Y, Corot C, Wendland MF, Daldrup-Link HE. (2006). T1 and T2 relaxivity of intracellular and extracellular USPIO at 1.5T and 3T clinical MR scanning. Eur Radiol, 16, 738–745.

Berry CC. (2005). Possible exploitation of magnetic nanoparticle-cell interaction for biomedical applications. J Mater Chem, 15, 543–547.

Ghavamzadeh R, Haddadi-Asl V, Mirzadeh H. (2004). Bioadhesion and biocompatibility evaluations of gelatin and polyacrylic acid as a crosslinked hydrogel *in vitro*. J Biomater Sci Polym Ed, 15, 1019–1031.